Synthesis of Nanoparticulate Alloys of the Composition Cu$_2$Zn$_{1−x}$Fe$_x$SnS$_4$: Structural, Optical, and Magnetic Properties

Punarja Kevin,[†] Mohammad Azad Malik,[‡] Simon Mcadams,[†] and Paul O'Brien*,[†,‡]

[†]School of Chemistry and [‡]School of Materials, The University of Manchester, Oxford Road, Manchester M13 9PL, U.K.

Ⓢ *Supporting Information*

ABSTRACT: Nanoparticles of the semiconductor Cu$_2$Zn$_{1−x}$Fe$_x$SnS$_4$ with different mole fractions of iron (x_{Fe}) were synthesized by the decomposition of molecular precursors in oleylamine. The composition, structure, optical, and magnetic properties of the nanoparticles are reported. The parent (Cu$_2$ZnSnS$_4$) zinc material is usually reported as kesteritic and the corresponding iron phase as stannitic; with different site occupancies and tetragonalities. In the small ca. 8–10 nm particles prepared, the smooth variation in lattice parameters and other measured properties suggest that the phase change, with composition, may be absent. SQUID magnetometry suggests that the iron containing samples are ferromagnetic at 5 K and paramagnetic at 300 K.

Photovoltaic cells based on stannitic phases such as Cu$_2$FeSnS$_4$ (CFTS) have demonstrated power conversion efficiency (PCE) of 8.03%[1] and devices prepared from Cu$_2$ZnSnS$_4$ (CZTS) nanoparticles annealed in Se atmosphere gave a PCE 7.2%.[2] Hydrazine processed (Cu$_2$ZnSn(S$_{1−x}$Se$_x$)$_4$) CZTSSe solar cells have demonstrated PCEs of up to 12.6%.[2] It has hence been shown that the efficiency of CZTS solar cells can be improved by addition of iron.[3,4] The ionic radius of Zn^{2+} and Fe^{2+} are 0.64 and 0.66 Å,[5] and Fe shows good solubility in the CZTS lattice; hence, Zn/Fe alloying is effective and allows ready access to solid state materials of the type Cu$_2$Zn$_x$Fe$_{1−x}$SnS$_4$ (0 > x > 1 CZFTS). As the Fe content in Cu$_2$Zn$_x$Fe$_{1−x}$SnS$_4$ increases, a structural transition from kesterite to stannite is usually seen.[6,7] At higher zinc content the electronic band gap increases because of the exchange and redistribution of electrons due to lower electronegativity of Zn (1.65) than Fe (1.83).[6] The band gap energies of post-sulfurized CZFTS films can be tuned from ~1.51 to 1.36 eV depending on Zn content (x = 0, 1 to 0).[8] The lattice parameters calculated for the CZFTS alloys show only small changes with composition as the radius of Zn(II) ion is very similar to that of Fe(II).[9]

CZFTS thin films have been deposited by spray pyrolysis followed by sulfurization[8] and pulsed laser deposition.[10] The magnetic properties,[11,12] Mössbauer spectra,[13] structural,[14,15] and vibrational characteristics[16] of CZFTS kesterite-stannite systems have been reported. A number of reports have appeared using molecular precursors for the preparation of nanoparticles or thin films of semiconductor materials.[17] We have recently reported the deposition of thin films of CZFTS by aerosol assisted chemical vapor deposition (AACVD).[18] Herein, we report the colloidal synthesis of Cu$_2$Zn$_{1−x}$Fe$_x$SnS$_4$ nanoparticles

using discrete molecular precursors. These materials are composed of comparatively cheap, abundant, and environmentally benign elements. The band gap can be tuned across the visible range, which makes them potentially useful in a variety of electronic, optoelectronic, and magneto electronic applications including solar energy harvesting. The magnetic properties are of interest as there are only a few studies[8,10,11,13,19] of such compounds especially in nanodispersed form.

The precursors used for the synthesis of CZFTS nanoparticles were [Cu(S$_2$CNEt$_2$)$_2$], [Zn(S$_2$CNEt$_2$)$_2$], [Fe(S$_2$CNEt$_2$)$_3$], and [^{n}Bu$_2$Sn(S$_2$CNEt$_2$)$_2$]. These metal−organic complexes were prepared by literature methods.[18,19] Initial screening experiments led to the selection of 220 °C and 1 h in oleylamine as good conditions for the reproducible preparation of nanocrystals (Supporting Information, Figure S1). The CZFTS samples were analyzed by energy dispersive X-ray (EDX) spectroscopy. An excellent correlation between the composition of the isolated materials and the mole fraction of the metal element (as a fraction of total metal in the solution) used for synthesis was observed. These results are summarized in Supporting Information (and Figure 1a, Table S1). The materials were analyzed by powder X-ray diffraction (p-XRD, Figure 1b). Figure S2 shows that selected *d*-spacings vary smoothly with the iron content of the material. The kesteritic to stannite transition has been discussed across the composition x_{Fe} = 0−1. The XRD analysis of CZFTS by Bonazzi[15] and the later neutron diffraction study by Schorr[6] are particularly useful in casting light on the complexity of the system.

Both of these reports give broadly similar lattice parameters for the two systems as a function of x_{Fe} and show a critical change in the ordering of the atoms and a phase change at x_{Fe} = 0.3. The neutron diffraction study suggests a slightly modified occupancy pattern for the zinc rich, kesteritic end of the series member involving disordering across all the metal sites except that of tin. The p-XRD patterns recorded in this study show only a limited number of peaks; such observations are common for small particles. However, phase identification is possible in such nanoparticles, and both CZTS and CFTS in a hexagonal form have been identified by crystallography.[20] Alivisatos et al. have demonstrated changes in the preferred form of CdTe nanocrystals with size.[21]

A least-squares method was used to index the peaks observed in the powder diffraction patterns by reference to standard patterns. The results of these calculations suggest that the tetragonality of the system is small and that the lattice parameter
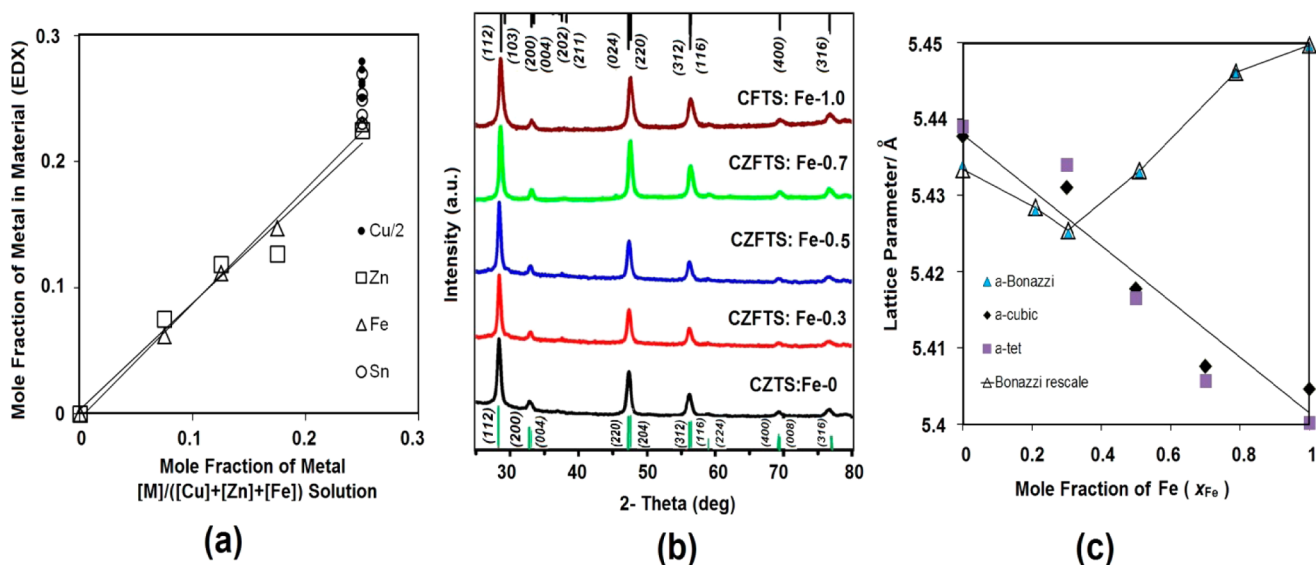
Figure 1. (a) Scatter plot showing the linear relationship between the mole fraction of metal in nanoparticles (by EDX) versus the mole fraction of metal (M) in the precursor mixture. (b) p-XRD patterns of CZFTS nanoparticles synthesized with increasing Fe/Zn ratios (220 °C, 1 h). Green and black stick patterns at the top and bottom of the panel are the standard patterns of CZTS (ICDD: 04−015−0223) and CFTS (ICDD: 04−015−0231). (c) Calculated and literature lattice parameters vs x_{Fe} for $Cu_2Zn_{1-x}Fe_xSnS_4$ nanoparticles.

a is similar to those of Bonazzi[15] and Schorr,[6] at low values of x_{Fe}. The monotonic decrease of a with increasing iron suggests that no phase change occurs in these small particles (Figure 1c). We have tested this model by indexing only the subset of data corresponding to the peaks we observed in the Bonazzi data sets.[15] Lattice constants a and c derived from this limited literature set are fully consistent with the results previously published and are overplotted in Figure 1c. In an interesting paper[7] Walsh et al. have shown that the a-values calculated by DFT for a kesteritic phase should decrease monotonically as the mole fraction of iron in the sample increases.[22] The d-spacings from the present samples change linearly with composition as is shown in Supporting Information Figure S2.

The morphologies and crystallinity of the CZFTS nanoparticles synthesized were investigated by high resolution transmission electron microscopy (HRTEM). The CZFTS nanoparticles were based on rhombohedra, whereas those of CFTS were oblate spheroids. A smooth transition was observed from one morphology to the other via hexagonal crystals at $x = 0.5$. All nanoparticles observed by TEM had a maximum length dimension in the range of ca. 9 ± 2 nm (Figure 2). The HRTEM images of the synthesized nanocrystals of $Cu_2Zn_{1-x}Fe_xSnS_4$ ($0 \geq x_{Fe} \geq 1$) (Figure 2) exhibit clear lattice fringes with measured d-spacing of 0.313(3), which can be assigned to the (112) lattice plane of the kesterite form.[20−23] These measured d-spacing also suggest that no phase change was occurring on changing the ratio of Zn to Fe; in agreement with the p-XRD results.

The analysis by EDX of atomic percentages in $Cu_2Zn_{1-x}Fe_xSnS_4$ nanoparticles showed the stoichiometric composition follows the amount of Fe in the precursor mixture as 26.4:11.4:0:12.9:49.3; 26.7:6.9:3.4:12.6:48.5; 29.8:6.3:6.0:13.3:44.6; 29.6:4.1:8.0:12.8:45.6; and 26.4:0:12.1:14.2:47.2, which give the stoichiometric formulas: $Cu_{2.3}Zn_{1.0}Fe_0Sn_{1.1}S_{4.3}$, $Cu_{2.7}Zn_{0.7}Fe_{0.3}Sn_{1.1}S_{4.7}$, $Cu_{2.4}Zn_{0.5}Fe_{0.5}Sn_{1.1}S_{3.6}$, $Cu_{2.4}Zn_{0.3}Fe_{0.7}Sn_{1.1}S_{3.8}$, and $Cu_{2.1}Zn_0Fe_{1.0}Sn_{1.2}S_{3.9}$, respectively (Supporting Information Table S1, Figure S3). An EDX elemental map showing the spatial distribution of the elements Cu, Zn, Fe, Sn, and S across a plane
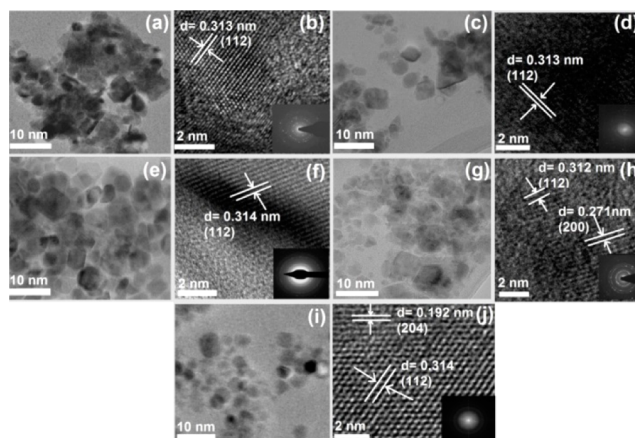

Figure 2. Bright-field TEM and HRTEM images for (a,b) CZTS ($x_{Fe} − 0$), (c,d) CZFTS ($x_{Fe} − 0.3$), (e,f) CZFTS ($x_{Fe} − 0.5$), (g,h) CZFTS ($x_{Fe} − 0.7$), and (i,j) CFTS ($x_{Fe} − 1.0$). Inset images show the selected area electron diffraction patterns of the same crystallites as in the associated bright field TEM and HRTEM images.

view of a sample of $Cu_2Zn_{1-x}Fe_xSnS_4$ ($x = 0.5$) was recorded (Supporting Information Figure S4) and demonstrates the homogeneity of the sample from the colocalization of the EDX signals for all elements analyzed. The composition of S was found to decrease with increasing Fe content, which agrees with other work.[8] Oxide phases can coexist with the sulfides that can compensate the sulfur deficiency in chalcogenide films.[8,24] The elemental analysis showed good control over the stoichiometry of the nanocrystals synthesized on varying the precursor composition for Zn and Fe. Figure 1a shows a linear correlation holds between the mole fractions of metal in feed and in the material formed.

X-ray photoelectron spectroscopy (XPS) was used to probe the chemical composition of the CZTS ($x = 0$), CFTS ($x = 1$), and $Cu_2Zn_{1-x}Fe_xSnS_4$ ($x = 0.5$) nanoparticles (Supporting Information Figures S5 and S6) and revealed the oxidation states of Cu, Sn, Zn, Fe, and Sn to be Cu^{1+}, Sn^{4+}, Zn^{2+}, Fe^{2+}, and $S^{2−}$.

The corresponding binding energies (BEs) for the Zn $2p_{3/2}$, Cu $2p_{3/2}$, Cu $2p_{1/2}$, Fe 2p, Fe $2p_{3/2}$, Fe $2p_{1/2}$, Sn $3d_{5/2}$, Sn $3d_{3/2}$, S $3p_{3/2}$, S $2p_{3/2}$, S $2p_{1/2}$, and S 2p are located at ∼1019, 9232, 953, 711, 710, 725, 482, 492, 156, 160, 170, and 174 eV, respectively.

The as-prepared CZFTS nanocrystals were dispersed in hexane and filtered to give clear, dark brown suspensions. The band gaps have been estimated by plotting $(Ah\nu)^2$ versus $h\nu$ ($A =$ absorbance, $h =$ Planck's constant, and $\nu =$ frequency) and extrapolating the linear portion of the plots in the band edge region; the method of Tauc.[24] The photoluminescence spectra of nanoparticles in the range 500−800 nm were recorded in hexane solvent after excitation at 400 nm. The values were (bandgap/eV, PL max/eV ($[x_{Fe}]/[x_{Fe}] + [x_{Zn}]$)): 1.93, 1.90 (0), 1.89, 1.82 (0.3), 1.87, 1.77 (0.5), 1.85, 1.74 (0.7), and 1.79. 1.9 (1.0), respectively (Supporting Information Figure S7a and Table S2). All PL spectra maxima (Supporting Information Figure S7b) are Stokes shifted to the red by ca. 0.5 eV as expected; quantum yields for all samples were of the order of 1%. These band gap associated measurements are all at higher energy than those observed for other CZFTS systems, suggesting quantum confinement.[8] A linear correlation was found between the PL and UV−vis spectroscopic results for the CZFTS nanoparticles (Supporting Information Figure S8). The band gap of the materials can hence be tuned across the visible spectrum by varying the composition of iron content in CZTS.

Typical results for CZFTS band gaps with increasing iron content include: films deposited by spray pyrolysis 1.51−1.33 eV,[8] pulsed laser deposition 1.74−1.33 eV,[10] and AACVD with the same precursors set as in the present work gave 1.72 eV (Zn-rich) to 1.67 (Fe- rich).[18] Walsh et al.[7] used DFT calculations and predicted band gaps of kesteritic CZTS and CFTS as 1.74 and 1.54 eV, respectively; the band gap of stannitic CZTS and CFTS are calculated as 1.36 and 1.85 eV, respectively.[7]

Magnetic studies were performed at 5 and 300 K for the Fe-containing samples. There are no such studies on the nanodispersed phases of these materials.[8,10,11,13,19] At 5 K, all samples displayed hysteresis, indicating ferromagnetic behavior[10,11] with coercive fields increasing from 260.63 Oe ($x = 0.3$) to 736.9 Oe ($x = 1.0$) $Cu_2Zn_{1-x}Fe_xSnS_4$, respectively (Figure 3a). Field-dependent magnetization curves revealed all samples as paramagnetic at 300 K, with magnetization increasing with Fe content (Figure 3b) as expected.[25,26] The zero-field-cooled (ZFC) and field-cooled (FC) magnetic measurements confirmed that 5 K is below the blocking temperature for all samples as is shown in Figure 3c.[10,11,13] Stannitic CFTS has a Neel temperature as low as 6−8 K.[26,27] The magnetic moments/BM calculated for the $Cu_2Zn_{1-x}Fe_xSnS_4$ nanoparticles ($[x_{Fe}]/[x_{Fe}] + [x_{Zn}]$) were 0.020792(0.3), 0.02846347 (0.5), 0.0358049(0.7), and 0.02502683(1.0), respectively, as compared to $Zn_{1-x}Fe_xS$ ($x = 0.4$) (0.00659 μ_B per Fe atom) and for $x = 0.6$. (0.00452 μ_B per Fe atom).[28] Dense nanograined ZnO thin films doped with iron (0 to 40 atom %) showed ferromagnetic behavior with Js up to 0.10 emu/g (0.025 μB/f.u.ZnO)[29] (see also Supporting Information Figure S9).

Nanoparticles of $Cu_2Zn_{1-x}Fe_xSnS_4$ with mole fractions of Fe (x_{Fe}) from 0 to 1 had been prepared. Detailed compositional studies based on the p-XRD patterns and EDX analysis showed that the material, in contrast to bulk, maintained a stannite structure. TEM studies showed slight differences in the structures and crystallinities of the nanoparticles with changes in composition of Fe (x_{Fe}). The iron containing materials were ferromagnetic at low temperatures. Such materials may find applications in magnetoelectronic, optoelectronic, or photo-
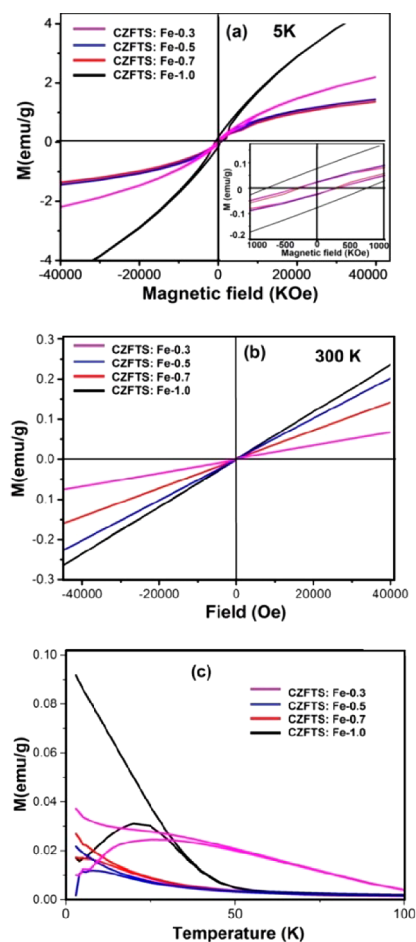

Figure 3. (a,b) Field-dependent magnetization curves of CZFTS nanocrystals at 5 K (inset: the magnification of typical hysteresis loops) and 300 K. (c) Temperature dependence of the magnetization for CZFTS ($x_{Fe} = -0.3$ to 1.0) nanocrystals.

voltaic applications. The fabrication of solar cells and devices using these relatively new nanoparticles are in hand and will be reported elsewhere.

◼ ASSOCIATED CONTENT

ⓢ Supporting Information

The Supporting Information is available free of charge on the ACS Publications website at DOI: 10.1021/jacs.5b10281.

> Experimental details, characterization of nanoparticles, p-XRD detailed interpretation, elemental maps, EDX analysis, and additional optical characterization (PDF)

◼ AUTHOR INFORMATION

Corresponding Author
*paul.obrien@manchester.ac.uk

Notes
The authors declare no competing financial interest.

◼ ACKNOWLEDGMENTS

■ REFERENCES

(1) Prabhakar, R. R.; Loc, N. H.; Kumar, M. H.; Boix, P. P.; Juan, S.; John, R. A.; Batabyal, S. K.; Wong, L. H. *ACS Appl. Mater. Interfaces* **2014**, *6*, 17661−17667.

(2) Guo, Q.; Ford, G. M.; Yang, W.-C.; Walker, B. C.; Stach, E. A.; Hillhouse, H. W.; Agrawal, R. *J. Am. Chem. Soc.* **2010**, *132*, 17384−17386. Wang, W.; Winkler, M. T.; Gunawan, O.; Gokmen, T.; Todorov, T. K.; Zhu, Y.; Mitzi, D. B. *Adv. Energy Mater.* **2014**, *4*, 1301465−1301471.

(3) Haight, R.; Barkhouse, A.; Gunawan, O.; Shin, B.; Copel, M.; Hopstaken, M.; Mitzi, D. B. *Appl. Phys. Lett.* **2011**, *98*, 253502−253507.

(4) Chen, S.; Walsh, A.; Yang, J.-H.; Gong, X. G.; Sun, L.; Yang, P.-X.; Chu, J.-H.; Wei, S.-H. *Phys. Rev. B: Condens. Matter Mater. Phys.* **2011**, *83*, 125201.

(5) Shannon, R. D.; O'Keeffe, M.; Navrotsky, A. *Ind. Chem. Libr.* **1981**, *2*, 53−70.

(6) Schorr, S.; Hoebler, H.-J.; Tovar, M. *Eur. J. Mineral.* **2007**, *19*, 65−73.

(7) Shibuya, T.; Goto, Y.; Kamihara, Y.; Matoba, M.; Yasuoka, K.; Burton, L. A.; Walsh, A. *Appl. Phys. Lett.* **2014**, *104*, 0219121−0219124.

(8) Khadka, D. B.; Kim, J. H. *J. Phys. Chem. C* **2014**, *118*, 14227−14237.

(9) Zeier, W. G.; Pei, Y.; Pomrehn, G.; Day, T.; Heinz, N.; Heinrich, C. P.; Snyder, G. J.; Tremel, W. *J. Am. Chem. Soc.* **2013**, *135*, 726−732.

(10) Agawane, G. L.; Shin, S. W.; Vanalakar, S. A.; Moholkar, A. V.; Kim, J. H. *Mater. Lett.* **2014**, *137*, 147−149.

(11) Bernardini, G. P.; Borrini, D.; Caneschi, A.; Benedetto, F. D.; Gatteschi, D.; Ristori, S.; Romanelli, M. *Phys. Chem. Miner.* **2000**, *27*, 453−461.

(12) Cui, Y.; Deng, R.; Wangm, G.; Pan, D. *J. Mater. Chem.* **2012**, *22*, 23136−23140.

(13) Benedetto, F. D.; Bernardini, G. P.; Borrini, D.; Lottermose, W.; Tippelt, G.; Amthauer, G. *Phys. Chem. Miner.* **2005**, *31*, 683−690.

(14) Kissin, S. A.; Reinvestigation, A. *Can. Miner.* **1989**, *27*, 689−697.

(15) Bonazzi, P.; Bindi, L.; Bernardini, G. P.; Menhetti, S. *Can. Mineral.* **2003**, *41*, 639−647.

(16) Fontane, X.; Izquierdo-Roca, V.; Saucedo, E.; Schorr, S.; Yukhymchuk, V.; Valakh, O.; Ya, M.; Perez-Rodriguez, A.; Morante, J. R. *J. Alloys Compd.* **2012**, *539*, 190−194.

(17) Malik, M. A.; Afzaal, M.; O'Brien, P. *Chem. Rev.* **2010**, *110*, 4417−4446.

(18) Kevin, P.; Malik, M. A.; O'Brien, P. *J. Mater. Chem. C* **2015**, *3*, 5733−5741.

(19) Ramasamy, K.; Malik, M. A.; O'Brien, P. *Chem. Sci.* **2011**, *2*, 1170.

(20) Zhang, X.; Bao, N.; Ramasamy, K.; Wang, Y.-H. A.; Wang, Y.; Lin, B.; Gupta, A. *Chem. Commun.* **2012**, *48*, 4956−4958.

(21) Manna, L.; Milliron, D. J.; Meisel, A.; Scher, E. C.; Alivisiatos, P. *Nat. Mater.* **2003**, *2*, 382−385.

(22) Personal Communication between Paul O'Brien, The University of Manchester, UK and Aron Walsh, University of Bath, UK.. Concerning future work on ref 7.

(23) Zheng, H.; Li, X.; Zong, K.; Sun, Y.; Liu, J.; Wang, H.; Yan, H. *Mater. Lett.* **2013**, *110*, 1−3.

(24) Tauc, J.; Grigorovici, R.; Vancu, A. *Phys. Status Solidi B* **1966**, *15*, 627−637. O'Leary, S. K.; Lim, P. K. *Solid State Commun.* **1997**, *104*, 17−21. Tauc, J. Optical Properties of Noncrystalline Solids. In *Optical Properties of Solids*; Abelks, F., Ed.; Elsevier: New York, 1972; pp 277−313. Meinert, M.; Reiss, G.; Tumuluri, A.; Naidu, K. L.; Raju, K. C. J. *Int. J. ChemTech Res.* **2014**, *6*, 3353−3356.

(25) Dixit, N.; Vaghasia, J. V.; Soni, S. S.; Sarkar, M.; Chavda, M.; Agrawal, N.; Soni, H. P. *J. Environ. Chem. Eng.* **2015**, *3*, 1691−1701.

(26) Bernardini, G. P.; Borrini, D.; Caneschi, A.; Benedetto, F. D.; Gatteschi, D.; Ristori, S.; Romanelli, M. *Phys. Chem. Miner.* **2000**, *27*, 453−455.

(27) Caneschi, A.; Cipriani, C.; Benedetto, F. D.; Sessoli, R. *Phys. Chem. Miner.* **2004**, *31*, 190−92.

(28) Parra-Palomino, A.; Perales-Perez, O.; Singhal, R.; Tomar, M.; Hwang, J.; Voyles, P. M. *J. Appl. Phys.* **2008**, *103*, 121−123.

(29) Straumal, B. B.; Protasova, S. G.; Mazilkin, A. A.; Tietze, T.; Goering, E.; Schutz, G.; Straumal, P. B.; Baretzky, B. *Beilstein J. Nanotechnol.* **2013**, *4*, 361−369. Rumpf, K.; Granitzer, P.; Morales, P. M.; Poelt, P.; Reissner, M. *Nanoscale Res. Lett.* **2012**, *7*, 445.